Functional Imaging and Modeling of the Heart (FIMH 2005)
A.F. Frangi et al. (Eds.)


# Analysis of the Interdependencies among Plaque Development, Vessel Curvature, and Wall Shear Stress in Coronary Arteries

Andreas Wahle[1], John J. Lopez[4], Mark E. Olszewski[1], Sarah C. Vigmostad[2], Krishnan B. Chandran[2], James D. Rossen[3], and Milan Sonka[1]

[1] Department of Electrical and Computer Engineering,
[2] Department of Biomedical Engineering,
[3] Department of Internal Medicine,
The University of Iowa, Iowa City, IA 52242, USA;
[4] Department of Medicine,
The University of Chicago, Chicago, IL 60637, USA.

andreas-wahle@uiowa.edu
http://www.engineering.uiowa.edu/~awahle

**Abstract.** The relationships among vascular geometry, hemodynamics, and plaque development in coronary arteries are not yet well understood. This in-vivo study was based on the observation that plaque frequently develops at the inner curvature of a vessel, presumably due to a relatively lower wall shear stress. We have shown that circumferential plaque distribution depends on the vessel curvature in the majority of vessels. Consequently, we studied the correlation of plaque distribution and hemodynamics in a set of 48 vessel segments reconstructed by 3-D fusion of intravascular ultrasound and x-ray angiography. The inverse relationship between local wall shear stress and plaque thickness was significantly more pronounced ($p<0.025$) in vessel cross sections exhibiting compensatory enlargement (positive remodeling) without luminal narrowing than when the full spectrum of vessel stenosis severity was considered. Our findings confirmed that relatively lower wall shear stress is associated with increased plaque development.

## 1 Introduction

Coronary atherosclerosis starts at a young age and is a major cause of death in developed countries. As shown in Fig. 1(a)–(c), the intimal layer (mid gray) thickens as plaque develops. However, the lumen (light gray) initially remains unchanged due to *compensatory enlargement* as part of a remodeling process that causes the media (dark gray) to grow outward. Luminal narrowing forming an angiographically visible stenosis generally occurs after the plaque area exceeds about 40% of the cross-sectional vessel area [1]. Intravascular ultrasound

Supported in part by the National Institutes of Health, grant R01 HL63373.

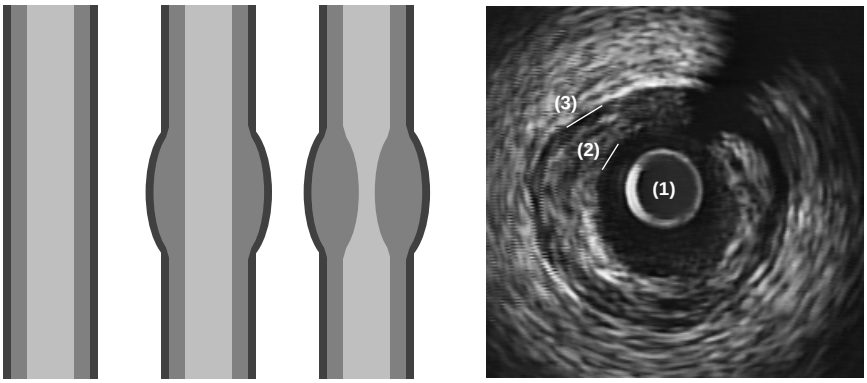


**Fig. 1.** Development of atherosclerotic plaque: (a) vessel without any stenosis; (b) compensatory enlargement; (c) luminal narrowing; (d) IVUS image with (1) catheter, (2) lumen/plaque, and (3) media/adventitia borders.

(IVUS) is able to visualize plaque development, as shown in Fig. 1(d). Previous studies have linked plaque development with low wall shear stress [2]. Thus, the identification of areas of initially low wall shear stress and evaluation of the plaque distribution is of major interest, especially given the capabilities of IVUS to image plaque. As is typical for coronary IVUS studies, all subjects imaged had clinically indicated coronary catheterization. It is imprudent to perform IVUS imaging in patients with healthy or minimally diseased coronary vessels. Consequently, the enrolled subjects invariably suffered from advanced coronary artery disease. As such, the relationships we observed were between an already substantially altered coronary morphology and the related altered hemodynamic shear stress conditions. It has been shown that luminal narrowing deminishes the inverse relationship between plaque thickness and wall shear stress [3]. In addition to this phenomenon, we were also interested in the notion that hemodynamic shear stress plays a role in the onset of coronary disease. In contrast to wall shear stress, vascular geometry (curvature) is not changed by the course of the disease and thus can serve as a surrogate of the hemodynamic conditions prior to atherosclerotic disease development. Therefore, the relationship between vessel curvature and plaque distribution was studied as well as the relationship between wall shear stress and plaque distribution with special consideration of vascular remodeling.

## 2 Methods

### 2.1 Multi-Modality Fusion

We have developed a comprehensive system that generates geometrically correct 3-D and/or 4-D (i.e., 3-D+time) reconstructions of coronary arteries and

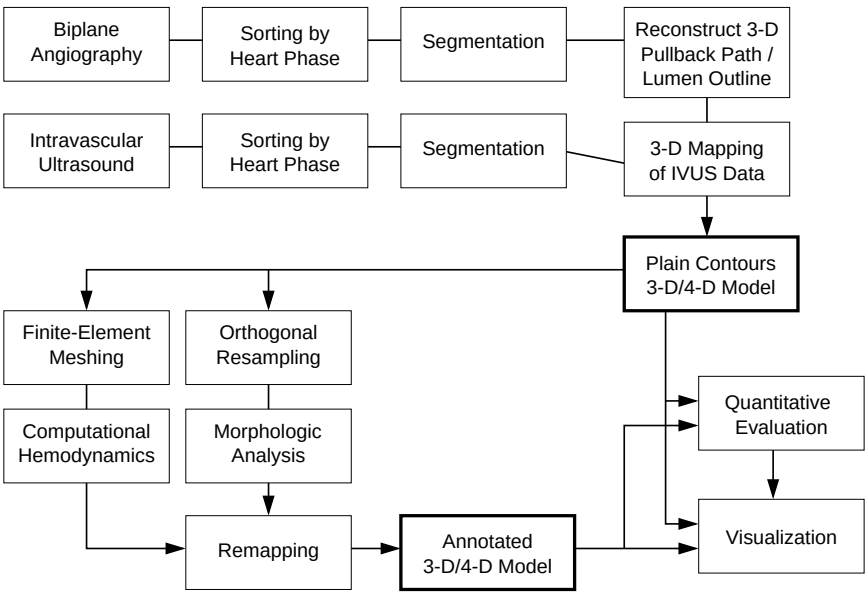


**Fig. 2.** Processing of the data as outlined in Section 2.1.

computes corresponding quantitative indices of coronary lumen and wall morphology. The reconstructions serve as input for hemodynamic analyses and allow for interactive visualization [4–6]. A flowchart outlining the system is given in Fig. 2. In brief, the vessel geometry is obtained from biplane (or a pair of single-plane) x-ray angiographic projections, whereas the cross-sectional information is retrieved from IVUS. Thus, the resulting model accurately reflects the curvature and torsion of the vessel as well as any accumulated plaque. The angiography and IVUS data are retrospectively ECG-gated and segmented. Fusion leads to the 3-D/4-D *plain model* representing both the lumen and the vessel wall. The model consists of the lumen/plaque and media/adventitia contours oriented relative to the IVUS catheter. After tetrahedral meshing, this model is suitable for hemodynamic analyses. Following resampling orthogonal to the vessel centerline, morphologic analyses are performed. The quantitative results *annotate* the resampled contour model, which is subsequently used for visualization and further analyses. Our system utilizes conventional PC hardware and widely available software tools. Standardized storage formats for parameters and contour lists have been adopted to ensure proper interfacing between our fusion system and commercially available analysis software packages and to enhance data sharing and collaboration.

## 2.2 Segmentation of IVUS Image Data

While many components of the fusion system perform to full satisfaction, several challenges remain. One of them is the segmentation of the IVUS data. It is well

known that IVUS images contain artifacts from various sources, thus requiring the design of cost functions that incorporate a-priori knowlegde of regional and border properties to robustly determine the optimum contours. The cost function employed in our graph-based IVUS segmentation method combines three major groups of features: (a) image data terms such as edge detectors and intensity patterns; (b) physics-based terms that distinguish different tissue types based on their Rayleigh distribution patterns [7, 8]; and (c) border probabilities based on expert tracings. A scoring system is employed to evaluate these feature classes in each image to be analyzed, and the borders are found using a multiresolution approach that mimics human vision [9].

### 2.3 Morphologic and Hemodynamic Indices

The reconstructed vascular model provides 3-D locations for 72 circumferential vertices on both lumen/plaque and media/adventitia contours, radially oriented with respect to the vessel centerline. This allows a straightforward determination of the plaque thickness at each location, as well as volumetric measurements over any given subsegment of the vessel [10]. In order to determine local curvature magnitude and direction, Frenet-based computational geometry was employed. To distinguish between locations of "inner" vs. "outer" curvature on the circumference of the vessel, a new scheme was introduced that weights the curvature magnitude by an index of the circumferential position of each element [11]. Blood flow through the coronary arteries was simulated using *computational fluid dynamics* (CFD) methodology. Tetrahedral meshing of the lumen using commercially available meshing software provides an unstructured grid for simulations with U$^2$RANS, a CFD software developed at The University of Iowa [12]. Positive and negative wall shear stress values are determined at each circumferential lumen location and mapped onto the 3-D model.

### 2.4 Classification of Circumferential Regions

Each of the 72 circumferential locations in each vessel cross section was categorized with respect to its relative plaque thickness (above or below average for this cross section), its location relative to the local vessel curvature (inner or outer curvature), and its wall shear stress (above or below cross-sectional average). In this way, eight different "regions" resulted. A ninth "neutral" region included those areas of curvature magnitude below a certain threshold that were eliminated from further analysis to avoid distortion of the results by noise. The following two studies correlate independently plaque distribution with curvature and wall shear stress.

## 3 Studies and Results

### 3.1 Plaque Distribution in Relation to Vessel Curvature

To verify the observation that plaque accumulation in curved vessels is biased towards the inner bend of the curvature rather than the outer bend of the cur-

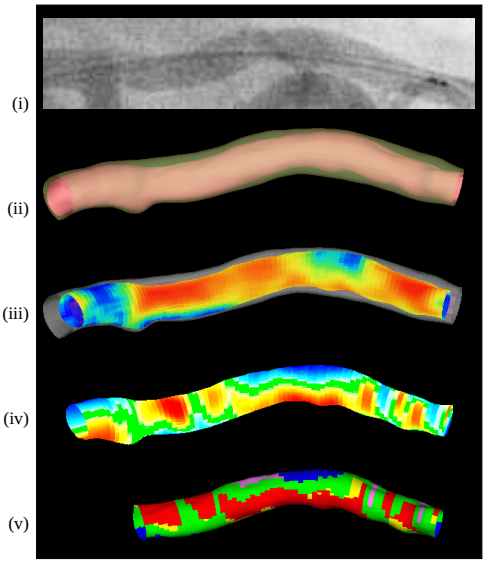


(a)

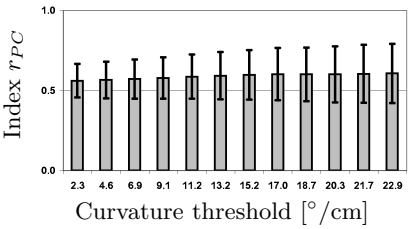


| $r_{PC}>0.5$ for $n$ thresholds | | | | | |
|---|---|---|---|---|---|
| *Vessel* | 12 | ≥6 | ≥1 | =0 | |
| LAD | 17 | 3 | 1 | 2 | *23* |
| RCA | 10 | 4 | 1 | 8 | *23* |
| LCX | 9 | 1 | 0 | 4 | *14* |
| | *36* | *8* | *2* | *14* | *60* |

(b)

**Fig. 3.** Plaque thickness vs. curvature: (a)(i) angiogram of a left anterior descending artery with the IVUS catheter inserted, (ii) lumen and adventitia borders from fusion, (iii) plaque-thickness annotation, (iv) curvature-index annotation, (v) after classification into regions, with the branch segment removed from analysis; (b) results from 60 analyzed vessels, by curvature threshold and vessel, with $r_{PC}>0.5$ indicating that our guiding hypothesis was satisfied for all (12), at least half (≥6), at least one (≥1), or none (=0) of the curvature thresholds.

vature, the relative amount $r_{PC}$ of regions where inner curvature coincides with above-average plaque accumulation, or outer curvature coincides with below-average plaque accumulation, was determined in a set of 60 vessels. Preliminary results in 37 vessels and methodology were reported in [11]. The ratio $r_{PC}$ represents a "plaque/curvature index" with a value $r_{PC}>0.5$ indicating that more plaque has accumulated along the inner curvature as compared to the outer curvature, thus supporting the hypothesis. As an example, Fig. 3(a)(iii) shows a color-coded plaque-thickness distribution in a geometrically correct 3-D representation, with red indicating high and blue indicating low plaque thickness, normalized over the entire vessel segment. As described above, a curvature index was determined for each circumferential location on the contour. Fig. 3(a)(iv) shows the color-coded curvature-index distribution, with red indicating inner curvature and blue indicating outer curvature. Four regions were defined, as depicted in Fig. 3(a)(v): $R_{ai}$ (red), $R_{ao}$ (magenta), $R_{bi}$ (yellow), and $R_{bo}$ (blue). These regions represent pairs distinguishing circumferentially considered "above-average" plaque thickness ($a$) from "below-average" plaque thickness ($b$), coinciding with either "inner curvature" ($i$) or "outer curvature" ($o$) of the vessel

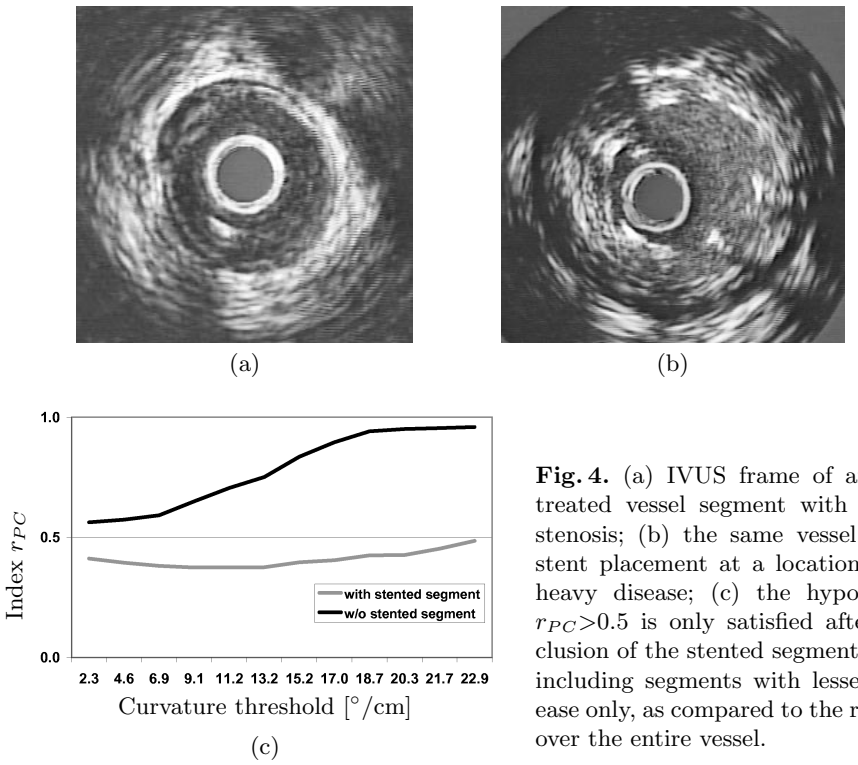


**Fig. 4.** (a) IVUS frame of an untreated vessel segment with slight stenosis; (b) the same vessel after stent placement at a location with heavy disease; (c) the hypothesis $r_{PC}$>0.5 is only satisfied after exclusion of the stented segment, thus including segments with lesser disease only, as compared to the results over the entire vessel.

wall. Thus, the plaque/curvature index was defined as

$$r_{PC} = \frac{\|R_{ai} + R_{bo}\|}{\|R_{ai} + R_{bo} + R_{ao} + R_{bi}\|} \tag{1}$$

**Impact of Curvature Threshold and Vessel Type.** The results are depicted in Fig. 3(b). Twelve different threshold values were empirically selected ranging from 2.31 to 22.94°/cm, resulting in 10.1–77.8% of circumferential locations being assigned to the neutral region $R_n$ (green). The chart shows that the average $r_{PC}$ over all 60 vessels increases steadily with increase of the curvature threshold. Thus, the more regions of low curvature are included into $R_n$, and therefore increasing the proportion of higher curvature regions included in the calculation of $r_{PC}$, the more the hypothesis was supported. The increase in standard deviation of $r_{PC}$ prompted us to categorize the results by vessel. While almost two thirds of the vessels satisfied $r_{PC}$>0.5 for *all* thresholds, the hypothesis was more strongly supported in left anterior descending (LAD) arteries (87% for all or at least half of the thresholds). Since the right coronary (RCA) and left circumflex (LCX) arteries have higher tortuosity than the LAD, the less supportive results may be caused by the more complex flow patterns that can no longer be explained by the curved-tube model.

**Impact of Interventions.** Stenting may have a substantial impact on the outcome of the plaque/curvature index $r_{PC}$. In several of the vessels analyzed, a below-threshold value of $r_{PC}$ ($r_{PC}$<0.5) was determined when all segments were included and only branch locations were excluded. After also excluding known regions of intervention and stenting, $r_{PC}$>0.5 was reached, frequently showing the increase of $r_{PC}$ with the increase in curvature threshold (Fig. 4). This contradicts our initial findings reported in [11] that stenting does not significantly affect the plaque/curvature index $r_{PC}$ and indicates that substantial disease and stenting *may* have a distorting impact on the relation between vessel geometry and plaque distribution.

### 3.2 Plaque Distribution in Relation to Wall Shear Stress

While disease progression and stenting impact the curvature/plaque relationship to some extent, an even more substantial effect can be expected on the wall shear stress distribution. The distribution is substantially altered when the limits of positive remodeling are reached [3]. Thus, the vessel subsegments for which the area stenosis is between 10% and 40% are of specific interest (the compensatory-enlargement range identified by Glagov et al. [1]). Consequently, we concentrated on whether and how significantly the correlation improves once vessel segments of certain properties are excluded from the analysis. In this way, indirect evidence of which local conditions favor the underlying hypothesis of below-average wall shear stress inducing above-average plaque thickness was sought.

**Grouping of Vessels and Segments by Disease Severity.** 48 vessels (a subset of Section 3.1, since some parameters were not available for vessels received from collaborating sites) were analyzed. The data was smoothed with a moving 45°-wedge over 5 frames to limit the impact of local noise. The analyses were performed in 4 increasingly restrictive subsets of data. First, the relative amount $r_{PW}$ of elements for which circumferentially above-average plaque thickness coincides with below-average wall shear stress (and vice versa) was determined for each vessel segment – similar to the plaque-thickness/curvature study. By replacing "inner curvature" ($i$) with "lower-than-average wall shear stress" ($l$) and "outer curvature" ($o$) with "higher-than-average wall shear stress" ($h$) in Eq. (1),

$$r_{PW} = \frac{\|R_{al} + R_{bh}\|}{\|R_{al} + R_{bh} + R_{ah} + R_{bl}\|} \tag{2}$$

results as definition for the plaque/wall-shear-stress index. This step created Set #1. Next, all vessel subsegments that included vessel branching areas, stents, or regions of dense calcification were excluded, forming Set #2. Within Set #2, percent-area stenosis was determined for each frame following Glagov's definition, which does not require the presence of a normal reference segment (plaque+wall area over cross-sectional vessel area) [1]. Set #3 consisted of all such vessles from Set #2 for which the percent-area stenosis was in the range of 10–40% in at least 35% of the non-excluded vessel segments. Set #3 consisted

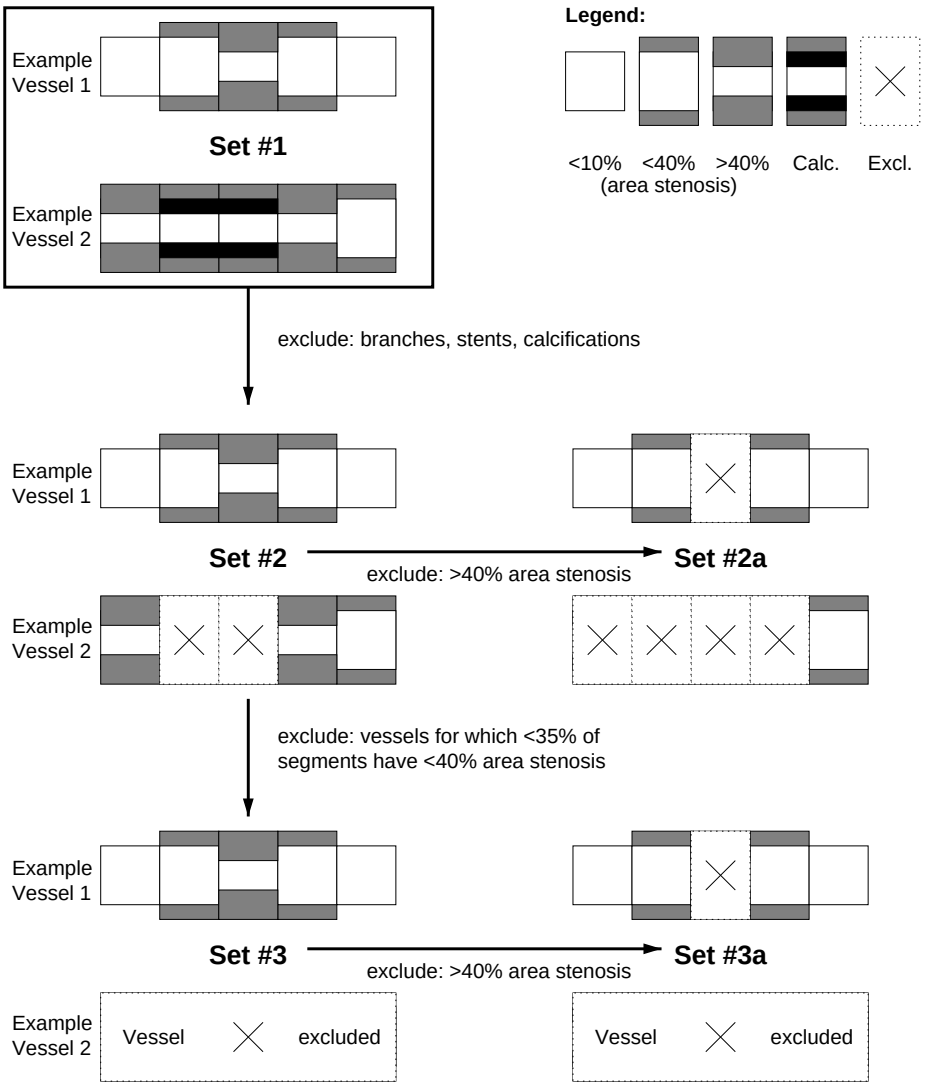


**Fig. 5.** Example for the definition of the sets: Vessel 1 shows only minor disease, whereas Vessel 2 is subject to advanced atherosclerosis; both form Set #1. For Vessel 1, all subsegments are retained when proceeding to Set #2, whereas two subsegments of Vessel 2 were discarded due to calcifications. All subsegments outside the 10–40% area stenosis range are removed from Set #2 to create Set #2a, thus discarding 1 subsegment from Vessel 1 and 2 subsegments from Vessel 2. Only Vessel 1 proceeds from Set #2 to Set #3, since less than 35% of Vessel 2 are within the 10–40% area stenosis range. For Vessel 1, (in analogy to the step from Set #2 to Set #2a) the center segment is discarded from Set #3 to Set #3a.

of 31 vessels satisfying this criterion. In each vessel, the segments of Sets #2 and #3 that were within the 10–40% range of area stenosis formed Subsets #2a and #3a. An illustration for the definition of these sets is shown in Fig. 5.

**Hypothesis Test.** If the hypothesis is correct and observable in regions where severe luminal narrowing is not present, the vessels in Subsets #2a and #3a should provide higher $r_{PW}$ ratios than the corresponding vessels in Sets #2 and #3. Therefore, we determined factors $g_{PW}$ quantifying the change $g_{PW\{2\}} = r_{PW\{2a\}}/r_{PW\{2\}}$ for all vessels and $g_{PW\{3\}} = r_{PW\{3a\}}/r_{PW\{3\}}$ for vessels with the minimum of 35% of frames within the 10–40% area-stenosis range. Note that the $g_{PW\{x\}}$ represent the differences in hypothesis validity. Consequently, $g_{PW\{x\}}>1$ suggests a case for which the hypothesis is more strongly supported in those segments of vessel $x$ with compensatory enlargement as compared to those with lumen narrowing. The analysis rationale is to determine: (1) whether applying the hypothesis test on the subset of segments defined in Set #2a (10–40% stenosis) increases the validity of the hypothesis compared to the Set #2; and, (2) whether applying the hypothesis test on Set #3a (10–40% stenosis in vessels with ≥35% of the wall within this range) increases the hypothesis validity compared to the Set #3 (≥35% of the wall within the 10–40% stenosis range).

**Changes in Hypothesis Validity.** The results can be summarized in the following table ($g_{PW\{x\}}\geq 1.01$ "increase" and $g_{PW\{x\}}\leq 0.99$ "decrease"):

| | $g_{PW\{x\}}$ | ≥1.01 | <1.01 >0.99 | ≤0.99 | * | |
|---|---|---|---|---|---|---|
| Sets #2a/#2 | *n=48* | 25 | 3 | 16 | 4 | $R$=0.61, $p$>0.75 |
| #3a/#3 | *31* | 19 | 3 | 7 | 2 | $R$=0.92, $p$<0.025 |

where for the vessels marked with ∗, either all or none of the frames were within the 10–40% area-stenosis range, therefore $g_{PW\{x\}}$ was considered undefined, and these vessels were excluded from the $R$ and $p$ calculations. Evidently, hypothesis validity improves and becomes statistically significant in Set #3 vs. Set #2, thus confirming our assumption. A notable cluster of 12 vessels in Set #3, having 35–63% of frames in the 10–40% area-stenosis range, shows an average 10.2% increase in hypothesis validity which is highly significant ($R$=0.96, $p$<0.001). This can be explained, in part, by the minimization of statistical noise with an even distribution of frames within vs. outside of the 10–40% area-stenosis range.

## 4 Discussion and Conclusions

Plaque development depends on the wall shear stress distribution, which in turn depends on the vessel geometry. The presented study demonstrated in-vivo that plaque distribution correlates with vessel curvature, and also correlates with wall shear stress in early stages of atherosclerosis. The analysis of a direct relationship between curvature and shear stress is ongoing. We have shown that, in the

majority of vessels, plaque tends to form at the inner curvature of the vessel wall. These findings suggest that low wall shear stress, which is typically associated with inner vessel curvature locations, likely contributes to the *initial* formation of atherosclerotic plaque in the early stages of the disease in human coronary arteries. However, the wall shear stress distribution is altered in the *later* stages of atherosclerosis, when positive remodeling can no longer compensate for the disease and the lumen narrows. We have demonstrated that the hypothesis of above-average plaque thickness being associated with below-average wall shear stress is more strongly supported in the *early* stages of disease progression.

## References

1. Glagov, S., Weisenberg, E., Zarins, C.K., Stankunavicius, R., Kolettis, G.J.: Compensatory enlargement of human atherosclerotic coronary arteries. New England Journal of Medicine **316** (1987) 1371–1375
2. Gibson, C.M., Diaz, L., Kandarpa, K., Sacks, F.M., Pasternak, R.C., et al.: Relation of vessel wall shear stress to atherosclerosis progression in human coronary arteries. Arteriosclerosis and Thrombosis **13** (1993) 310–315
3. Wentzel, J.J., Janssen, E., Vos, J., Schuurbiers, J.C.H., Krams, R., et al.: Extension of increased atherosclerotic wall thickness into high shear stress regions is associated with loss of compensatory remodeling. Circulation **108** (2003) 17–23
4. Wahle, A., Prause, G.P.M., DeJong, S.C., Sonka, M.: Geometrically correct 3-D reconstruction of intravascular ultrasound images by fusion with biplane angiography — Methods and validation. IEEE Transactions on Medical Imaging **18** (1999) 686–699
5. Olszewski, M.E., Wahle, A., Medina, R., Mitchell, S.C., Sonka, M.: Integrated system for quantitative analysis of coronary plaque via data fusion of biplane angiography and intravascular ultrasound. In Lemke, H.U., et al., eds.: Computer Assisted Radiology and Surgery, Amsterdam, Elsevier (2003) 1117–1122
6. Wahle, A., Olszewski, M.E., Sonka, M.: Interactive virtual endoscopy in coronary arteries based on multi-modality fusion. IEEE Transactions on Medical Imaging **23** (2004) 1391–1403
7. Burckhardt, C.B.: Speckle in ultrasound B-mode scans. IEEE Transactions on Sonics and Ultrasonics **25** (1978) 1–6
8. Wagner, R.F., Smith, S.W., Sandrick, J.M., Lopez, H.: Statistics of speckle in ultrasound B-scans. IEEE Transactions on Sonics and Ultrasonics **30** (1983) 156–163
9. Olszewski, M.E., Wahle, A., Mitchell, S.C., Sonka, M.: Segmentation of intravascular ultrasound images: A machine learning approach mimicking human vision. In Lemke, H.U., et al., eds.: Computer Assisted Radiology and Surgery, Amsterdam, Elsevier (2004) 1045–1049
10. Medina, R., Wahle, A., Olszewski, M.E., Sonka, M.: Three methods for accurate quantification of plaque volume in coronary arteries. International Journal of Cardiovascular Imaging **19** (2003) 301–311
11. Wahle, A., Olszewski, M.E., Vigmostad, S.C., Medina, R., Coşkun, A.Ü., et al.: Quantitative analysis of circumferential plaque distribution in human coronary arteries in relation to local vessel curvature. In: Proc. 2004 IEEE International Symposium on Biomedical Imaging, Piscataway NJ, IEEE Press (2004) 531–534
12. Lai, Y.G., Przekwas, A.J.: A finite-volume method for fluid flow simulations with moving boundaries. Computational Fluid Dynamics **2** (1994) 19–40